

See discussions, stats, and author profiles for this publication at: <https://www.researchgate.net/publication/51579598>

Hydrogenation of arenes and N-heteroaromatic compounds over ruthenium nanoparticles on poly(4-vinylpyridine): A versatile catalyst operating by a substrate-dependent dual site mech...

ARTICLE *in* DALTON TRANSACTIONS · AUGUST 2011

Impact Factor: 4.2 · DOI: 10.1039/c1dt10801h · Source: PubMed

CITATIONS

30

READS

32

3 AUTHORS, INCLUDING:



[Roberto Sánchez-Delgado](#)

City University of New York - Brooklyn College

117 PUBLICATIONS 3,428 CITATIONS

SEE PROFILE

This article is published as part of the *Dalton Transactions* themed issue entitled:

Dalton Transactions 40th Anniversary

Guest Editor Professor Chris Orvig, Editorial Board Chair
University of British Columbia, Canada

Published in issue 40, 2011 of *Dalton Transactions*

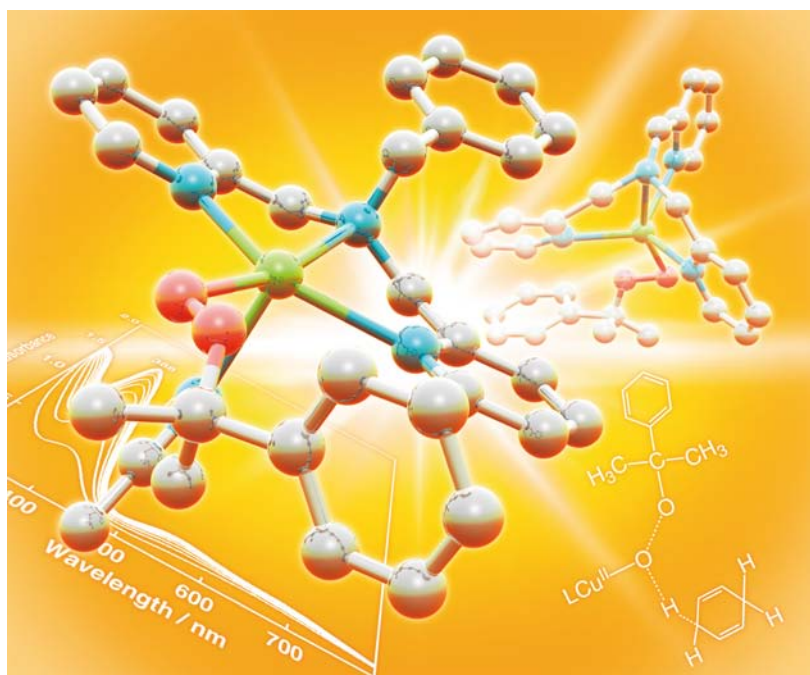


Image reproduced with permission of Shinobu Itoh

Welcome to issue 40 of the 40th volume of *Dalton Transactions*-40/40! Articles in the issue include:

PERSPECTIVE:

Synthesis and coordination chemistry of macrocyclic ligands featuring NHC donor groups

Peter G. Edwards and F. Ekkehardt Hahn
Dalton Trans., 2011, 10.1039/C1DT10864F

FRONTIER:

The future of metal–organic frameworks

Neil R. Champness
Dalton Trans., 2011, DOI: 10.1039/C1DT11184A

ARTICLES:

Redox reactivity of photogenerated osmium(II) complexes

Jillian L. Dempsey, Jay R. Winkler and Harry B. Gray
Dalton Trans., 2011, DOI: 10.1039/C1DT11138H

Molecular squares, cubes and chains from self-assembly of bis-bidentate bridging ligands with transition metal dications

Andrew Stephenson and Michael D. Ward
Dalton Trans., 2011, DOI: 10.1039/C1DT10263J

Visit the *Dalton Transactions* website for more cutting-edge inorganic and organometallic research

www.rsc.org/dalton

Hydrogenation of arenes and N-heteroaromatic compounds over ruthenium nanoparticles on poly(4-vinylpyridine): a versatile catalyst operating by a substrate-dependent dual site mechanism†

Minfeng Fang, Nataliya Machalaba and Roberto A. Sánchez-Delgado*

Received 30th April 2011, Accepted 23rd June 2011

DOI: 10.1039/c1dt10801h

A nanostructured catalyst composed of Ru nanoparticles immobilized on poly(4-vinylpyridine) (PVPy) has been synthesized by NaBH_4 reduction of $\text{RuCl}_3 \cdot 3\text{H}_2\text{O}$ in the presence of the polymer in methanol at room temperature. TEM measurements show well-dispersed Ru nanoparticles with an average diameter of 3.1 nm. Both powder XRD patterns and XPS data indicate that the Ru particles are predominantly in the zerovalent state. The new catalyst is efficient for the hydrogenation of a wide variety of aromatic hydrocarbons and N-heteroaromatic compounds representative of components of petroleum-derived fuels. The experimental data indicate the existence of two distinct active sites in the nanostructure that lead to two parallel hydrogenation pathways, one for simple aromatics involving conventional homolytic hydrogen splitting on Ru and a second one for N-heteroaromatics taking place *via* a novel heterolytic hydrogen activation on the catalyst surface, assisted by the basic pyridine groups of the support.

1. Introduction

Despite recent advances in the development of energy sources different from petroleum, conventional fuels—notably diesel and gasoline—will continue to dominate transportation markets for decades¹ and therefore new or improved methods for producing higher-quality, environmentally less harmful fossil fuels are highly desirable. Current legislation imposes severe limits on the amount of aromatics, sulfur and nitrogen in transportation fuels, something difficult to achieve with current refining technologies.² Considering the current levels of oil consumption, it is likely that light crude reserves will be exhausted in the foreseeable future and refinery feeds will increasingly consist of heavy and extra heavy petroleum and bitumens, which contain a higher proportion of large polycyclic hydrocarbons, together with N- and S-heteroaromatics, all of which need to be removed or transformed in order to maximize the yields of useful products and avoid catalyst poisoning.^{2,3}

Catalytic hydrogenation of polycyclic aromatics is an important alternative to upgrade heavy feedstocks into synthetic crudes. Removal of nitrogen and sulfur is routinely achieved through hydrodenitrogenation (HDN) and hydrodesulfurization (HDS) processes, both of which involve hydrogenation of aromatic and

heteroaromatic rings as key steps of complex reaction schemes, commonly promoted by sulfided Co–Mo, Ni–Mo and Ni–W catalysts.^{2,4} Nevertheless, metal sulfide catalysts require the use of high temperatures and pressures (300–400 °C, 50–100 bar) and only reduce a moderate proportion of aromatics due to thermodynamic limitations under normal operation conditions.⁵ Supported noble metal catalysts can function at lower temperatures far from equilibrium conditions but they are often poisoned by small amounts of S- or N-containing compounds present in refinery feeds.^{2–5} Therefore a need exists for new efficient catalysts capable of promoting the hydrogenation of aromatic compounds under moderate reaction conditions while not being susceptible to deactivation by the substrates, products or impurities present in the feeds.

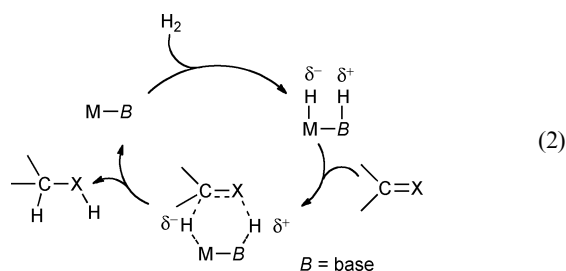
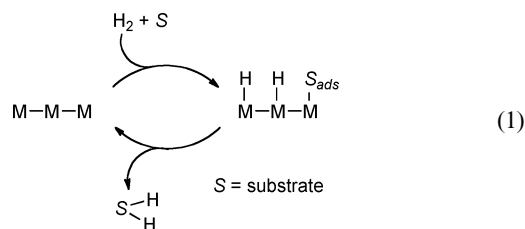
The use of nanoparticles (NPs) in catalysis continues to attract attention because of advantageous activity and selectivity features associated with the small particle size.^{6,7} A number of Ru NP-derived catalysts have been reported for the hydrogenation of arenes^{8–30} and, to a lesser extent, of N-heteroaromatic rings;^{18,23,31} Ru NPs have been utilized unsupported^{8–14} or ligand-stabilized^{15,16} in suspension in organic solvents, water or ionic liquids, and supported on polymers,^{17,18} inorganic oxides,^{19–23} or a combination of both.^{24,25} The role of the support has been most frequently to avoid aggregation of the particles and to facilitate catalyst recovery and recycling, although other effects, such as acidity, porosity or electron transfer processes have been claimed to influence activity and/or selectivity.^{32–34}

Concerning hydrogenation mechanisms, the most widely accepted pathway on solid catalysts involves the homolytic splitting of hydrogen molecules into hydrogen atoms on the metal surface,

Chemistry Department, Brooklyn College and The Graduate Center, The City University of New York (CUNY), 2900 Bedford Avenue, Brooklyn, NY, 11210, United States. E-mail: Rsdelgado@brooklyn.cuny.edu; Fax: +1-718-951-4607; Tel: +1-718-951-5000 ext. 2827

† Electronic supplementary information (ESI) available: Schematic illustration of TEM sample preparation; TEM, powder XRD and XPS data for used samples of Ru/PVPy catalyst. See DOI: 10.1039/c1dt10801h

followed by transfer to the chemisorbed substrate (eqn (1)).^{35,36} The intimate details of how these steps take place depend on the specific composition and structure of the catalyst. An interesting alternative pathway is the heterolytic splitting of H_2 into H^+ and H^- ; such mechanisms (eqn (2)) are common in solution, using either an external base or a ligand that contains basic sites.³⁷ Notable examples of this type of hydrogenation are Noyori's catalysts *e.g.* $RuH(diphosphine)(H_2N-CH_2-CH_2-NH)$, which



achieve very high activities and selectivities in the hydrogenation of $C=O$ and $C=N$ bonds, particularly in the case of prochiral substrates when a chiral version of the catalyst is employed.^{38,39} Heterolytic splitting of hydrogen is followed by an outer sphere concerted transfer of H^- and H^+ to the polar bond being hydrogenated, so that the substrate does not bind directly to the active metal center (eqn (2)).⁴⁰

Heterolytic hydrogen activation has been envisaged as a possible reaction pathway on metal sulfide catalysts,^{4,41} but evidence for such mechanisms remains extremely scarce for supported metal catalysts. NMR evidence for the formation of $Ru-H^-$ and $S-H^+$ upon reaction of RuS with H_2 has been presented;⁴² however, there are, to our knowledge, no mechanistic studies on supported metal nanoparticles promoting ionic hydrogenation pathways. We hypothesize that if a Noyori-type transition state (eqn (2)) can operate on a surface, poisoning effects can be minimized, since neither the substrate nor the products would enter into a strong direct interaction with the active metal sites. A possible way to favor heterolytic hydrogen splitting and ionic hydrogenation pathways on a solid catalyst is thus to create a nanostructure composed of small metal particles surrounded by basic functionalities provided by the support. Here we describe such a new catalyst composed of ruthenium nanoparticles supported on poly(4-vinylpyridine) ($Ru/PVPy$), which has proved to be a very versatile system for the hydrogenation of a variety of mono- and polynuclear arenes and nitrogen-containing aromatics. Our results suggest that the catalyst functions through two parallel mechanisms, depending on the substrate employed: a conventional one for simple aromatics and a second one involving novel ionic hydrogenation pathways in the case of N-heterocyclic substrates. We have disclosed some preliminary data indicating that the hydrogenation of quinoline over $Ru/PVPy$ takes place *via* ionic pathways.⁴³

2. Results and discussion

2.1. Catalyst design and preparation

Our working hypothesis is that the combination of small metal particles with basic functionalities provided by the support will lead to a nanostructure capable of promoting the heterolytic splitting of hydrogen and ionic hydrogenation mechanisms.

The metal of choice in this case was ruthenium, because of its known hydrogenation ability. Poly(4-vinylpyridine) (2% cross-linked with divinylbenzene) was selected as the support because the pyridine units have strong affinity for metals and also provide the adjacent basic sites required to produce our desired nanostructure. Furthermore, this resin is insoluble in all common solvents and highly resistant to degradation by temperature or strongly acidic or basic media. Fig. 1 shows a representation of the proposed nanostructure of our catalyst $Ru/PVPy$.

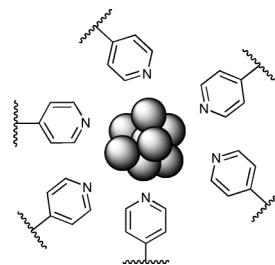


Fig. 1 Schematic representation of the proposed nanostructure for the $Ru/PVPy$ catalyst.

The $Ru/PVPy$ material containing 10 wt% metal was prepared by reduction of $RuCl_3 \cdot 3H_2O$ with $NaBH_4$ in methanol in the presence of the polymer support; the formation of the nanoparticles and their attachment to the polymer was followed by the discoloration of the solution and the darkening of the solid. The completeness of the reaction was verified by the lack of any UV-vis bands of the final solution, other than those ascribed to the solvent. The catalyst was routinely stored under nitrogen but quickly weighed in the air.

2.2. Catalyst characterization

2.2.1. TEM studies. Samples for TEM were prepared by mixing powdered $Ru/PVPy$ with epoxy resin in a brass tube, curing it at 150 °C and cutting the filled tube into thin disks, which were subjected to flat grinding, followed by dimple grinding and ion-milling to perforation to obtain electron transparent areas less than 100 nm thick (see Experimental section and Scheme S1, ESI†).

Fig. 2 shows a typical TEM image of a freshly prepared catalyst, which reveals a very narrow particle size distribution with an average particle size of 3.1 nm. The TEM image of a used catalyst recovered after hydrogenation of toluene at 120 °C under 10 bar (Fig. S1, ESI†) shows that the average Ru particle size exhibits a moderate increase to 4.9 nm after a catalytic run, which indicates a reasonable stability under typical reaction conditions.

2.2.2. XRD analysis. Fig. 3 depicts the XRD pattern observed for a freshly prepared sample of $Ru/PVPy$. Diffuse peaks were observed as expected for a homogeneous distribution of very

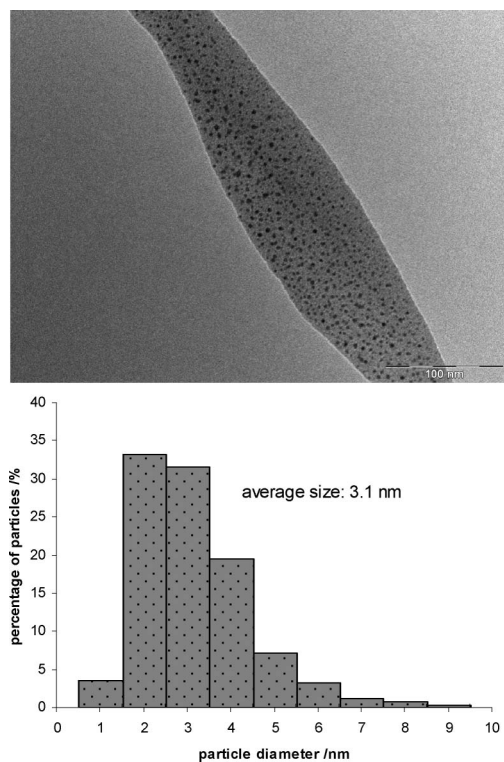


Fig. 2 Transmission electron micrograph of a fresh sample of Ru/PVPy with the corresponding size distribution histogram for Ru nanoparticles.

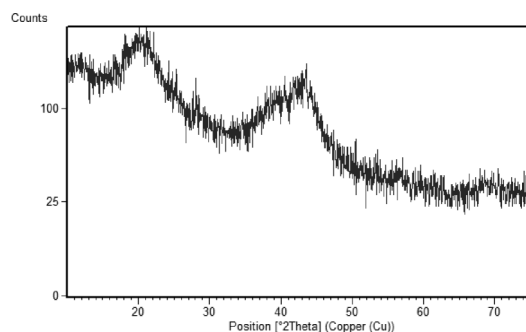


Fig. 3 Powder XRD diffraction pattern of a fresh sample of Ru/PVPy.

small metal particles; the diffraction angle of the peak at 44° is consistent with the d value (2.06 \AA) due to the (101) plane of Ru metal,⁴⁴ allowing us to characterize the particles as metallic Ru. No RuO_2 diffraction peaks were observed in the whole range of the diffractogram. The diffuse peak at 21° corresponds to the polymeric support. After a quinoline hydrogenation run at 120°C under 10 bar, the XRD pattern of the recovered catalyst is essentially identical to that of the fresh catalyst, confirming that the oxidation state and the structure of the Ru nanoparticles remains unchanged after a hydrogenation reaction (Fig. S2, ESI†).

2.2.3. XPS studies. In order to further establish the nature of the Ru nanoparticles, X-ray photoelectron spectroscopy (XPS) measurements were performed on a fresh catalyst and a used catalyst recovered from hydrogenation of quinoline at 150°C and 50 bar of H_2 .

In the survey scans of both samples (Fig. 4), Ru 3p, 3d and 4p peaks, O 1s, N 1s and C 1s peaks were observed, located at around

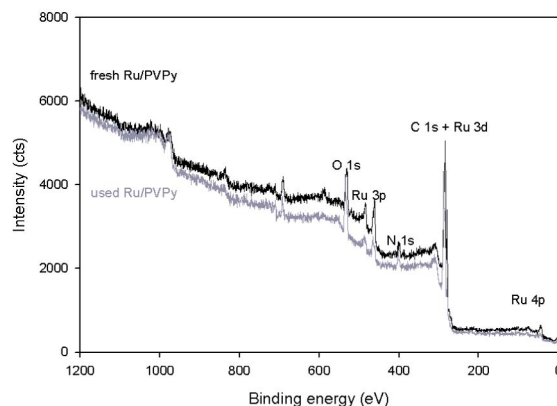


Fig. 4 XPS survey scans of a fresh and a used sample of Ru/PVPy after a hydrogenation run (substrate: quinoline, 150°C and 50 bar, in THF).

490–460, 280–290 and 43–46, 530, 400 and 288 eV, respectively. No B or Cl peaks were observed around 188 eV (B 1s), 200–202 eV (Cl 2p) and 270 eV (Cl 2s).⁴⁵

The narrow scan spectra within the Ru 3d region show highly overlapping Ru 3d peaks and C 1s peaks (Fig. 5). At least six component peaks are necessary to fit the experimental peaks for both fresh and used catalyst samples: Ru(0) $3d_{5/2}$ and $3d_{3/2}$, Ru(IV) $3d_{5/2}$ and $3d_{3/2}$, and C 1s peaks. The C 1s experimental peak at around 284.5 eV is too complicated to deconvolve: it has contributions from at least three different types of carbon (C–C, C=C and C=N) of the poly(4-vinylpyridine) support, with binding energies of 285.0, 285.5 and 286 eV, respectively,⁴⁶ plus carbonaceous contaminants such as CH_x species accumulated on the catalyst surface. Since the carbon peaks are not of particular relevance to our discussion, only a single contributing peak was applied for simplicity. A further C 1s experimental peak at around 287 eV can be attributed to C–O bonds,⁴⁵ most likely due to residual methanol from the synthesis adsorbed on the catalyst surface. After a quinoline hydrogenation run, the relative intensity of both C 1s peaks was increased (Fig. S3, ESI†); these signals can be attributed to adsorbed organic material containing C–O and C–N bonds, including THF, quinoline and/or its hydrogenation products.

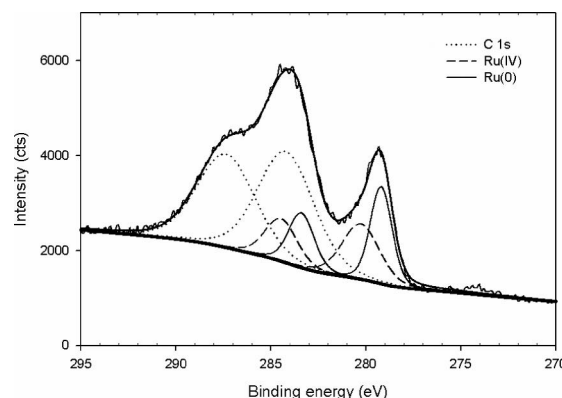


Fig. 5 C 1s and Ru 3d XPS spectra of a fresh sample of Ru/PVPy.

Of more interest for our purposes, the peaks at 279.2 eV and 279.3 eV (Fig. 5) are assigned to Ru $3d_{5/2}$ spin–orbit components in the zerovalent state, whose binding energies are generally given

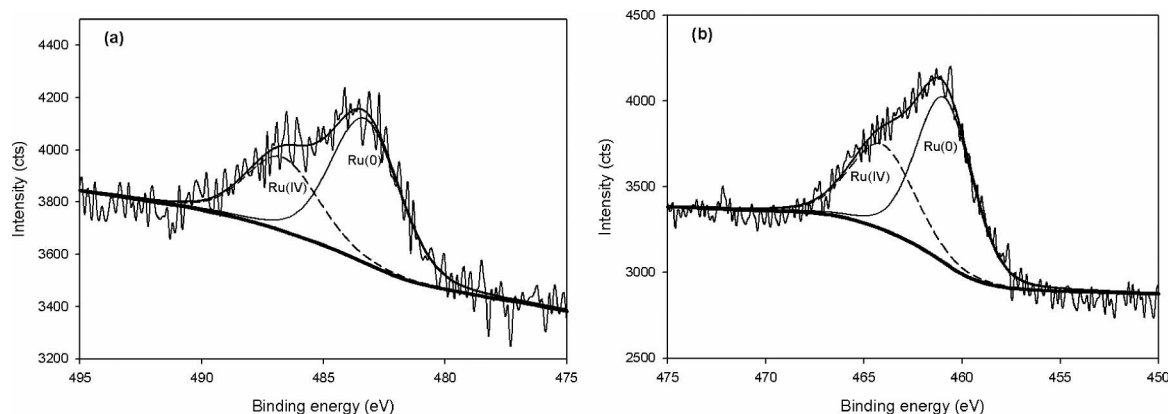


Fig. 6 3p XPS spectra of a fresh sample of Ru/PVPy: (a) $3p_{1/2}$; (b) $3p_{3/2}$.

as 280.1 eV for pure Ru metal.⁴⁵ The Ru $3d_{3/2}$ binding energies for both samples were observed at about 283.4 eV, which are also lower than that of bulk Ru metal (284.2 eV). The negative shift of the Ru 3d core level binding energies (about 0.8 eV) with respect to that of the standard metallic Ru is possibly derived from the strong interaction of the Ru particles with the N atoms of the PVPy, resulting in an electron density transfer from the basic support to the metallic particles. Similar effects have been observed for Ru metal particles supported on magnesia.^{47,48} Finally, the separation of the Ru 3d peaks is 4.2 eV, consistent with the Ru 3d spin–orbit splitting value.⁴⁹ The presence of a Ru(IV) component in both fresh and used catalyst probably results from air exposure during sample preparation and we believe that the Ru nanoparticles involved in the hydrogenation reactions are predominantly in the zerovalent state.

In the narrow scan spectra within the Ru 3p region, the experimental curve for the fresh catalyst is well-fitted by a main signal with maxima at 483.3 and 460.9 eV (Fig. 6), which corresponds to the binding energy of Ru $3p_{1/2}$ and Ru $3p_{3/2}$ of Ru(0), respectively. An additional signal at higher energies (486.7 and 464.1 eV) is attributed to a Ru(IV) component. The binding energy of Ru $3p_{3/2}$ (460.9 eV) is also lower than that of standard Ru metal (461.5 eV), consistent with the negative shift of the Ru 3d core level spectrum and due to the ability of the basic polymer support to donate electrons to the surface Ru metal atoms. For the used catalyst at least two contributing peaks in both the Ru $3p_{1/2}$ and $3p_{3/2}$ regions are necessary to fit the experimental bands (Fig. S4, ESI†). The peaks at 483.3 eV in the $3p_{1/2}$ region and 461.1 eV in the $3p_{3/2}$ region correspond to Ru(0), in agreement with the data for fresh catalyst. However, the peaks at 487.5 eV and 464.9 eV both show a positive shift of 0.8 eV compared to the peaks assigned to RuO₂ in fresh catalyst, and the relative intensities also increase significantly. These peaks can be assigned more likely to Ru atoms bonding to O or N atoms of residual organic material from hydrogenation reactions, in agreement with the increase in peak intensities observed in the C 1s region for the used catalyst (Fig. S3, ESI†).

2.3. Catalytic hydrogenation

2.3.1. Hydrogenation of arenes. The Ru/PVPy catalyst efficiently hydrogenates a variety of aromatic compounds under moderate reaction conditions. Blank tests under analogous reaction conditions revealed no hydrogenation activity for the polymer sup-

port alone. The substrate disappearance and product appearance, measured by GC-MS, were converted into hydrogenation rates reported as TOF values.[‡] All hydrogenation runs were repeated at least twice in order to ensure reproducibility of the results and average TOF values are reported.

2.3.1.1. Hydrogenation of toluene. Toluene is exclusively hydrogenated to methylcyclohexane in the presence of Ru/PVPy at 120 °C and 10 bar H₂ (Table 1, entry 2). As shown in Fig. 7a, the hydrogenation profile is linear up to 80% conversion, providing a TOF value of 82 h^{−1}.

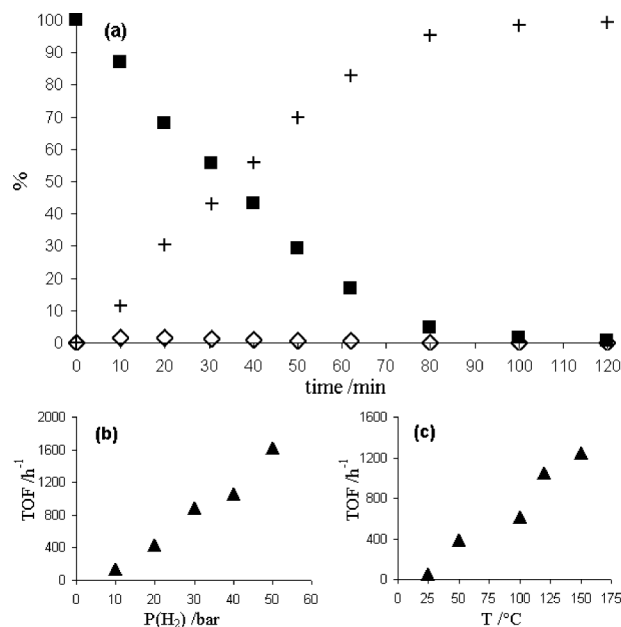
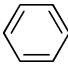
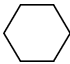
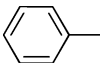
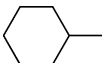
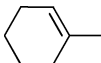
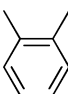
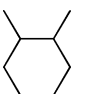
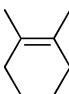
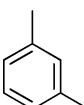
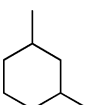
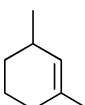
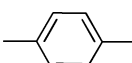
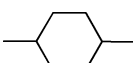
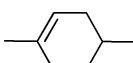
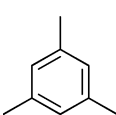
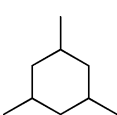
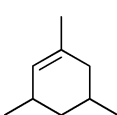
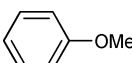

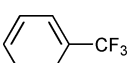
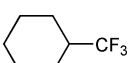
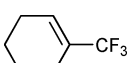


Fig. 7 (a) Hydrogenation of toluene over Ru/PVPy ($n_{\text{tol}}:n_{\text{Ru}} = 100$; 120 °C, 10 bar; in THF; ■: toluene; +: methylcyclohexane; ◇: methylcyclohexene); (b) influence of pressure on hydrogenation rate; (c) effect of temperature on hydrogenation rate.

Fig. 7b depicts the influence of the hydrogen pressure on the hydrogenation rate; within the range of 10–50 bar TOF values

[‡] TOF is defined as moles of *aromatic substrate converted* per mol of Ru per h. Some authors define TOF as *moles of hydrogen consumed* per mol cat per unit time. In this paper, all TOF values have been adjusted to our definition for comparison purposes.

Table 1 Hydrogenation of monocyclic aromatic hydrocarbons (MAHs) over Ru/PVPy^a

Entry	Substrate	TOF (h ⁻¹)	Product distribution at 1 h		
			Major		Minor
1		120		100%	—
2		69		99%	 1%
3		24		79%	 21%
4		23		81%	 19%
5		16		71%	 29%
6		3		62%	 38%
7 ^b		40		90%	10%
8		37		78%	22%
9		56		98%	 2%

^a In THF; $n_{\text{sub}} : n_{\text{Ru}} = 100$; 120 °C, 10 bar H₂; ^b 150 °C, 50 bar H₂.

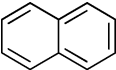
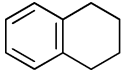
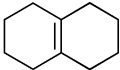
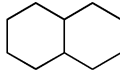
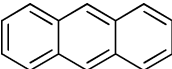
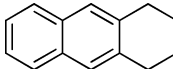
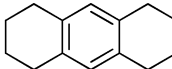
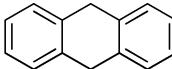
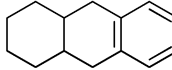
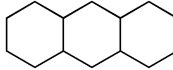
increase steadily with pressure, in contrast with our results for the hydrogenation of quinoline (*vide infra*), where a maximum optimal pressure was observed.⁴³ This indicates that sintering or other deactivation processes do not take place to an important extent on our catalyst at H₂ pressures of up to 50 bar. The hydrogenation rates for toluene, as expected, also increase with increasing temperature in the range 25–50 °C as depicted in Fig. 7c, showing that the catalyst is stable within this temperature range. Under the combined maximum temperature and pressure within our experimental range (150 °C and 50 bar H₂), toluene could be hydrogenated with a TOF of about 2000 h⁻¹. A number of other supported Ru catalysts are known to hydrogenate toluene, with TOF values ranging from *ca.* 100–1000 h⁻¹ under moderate conditions^{10,11,17,23,26,27} and 10,000–30,000 h⁻¹ at elevated temperature and pressure.^{19,24}

2.3.1.2. Hydrogenation of other arenes. In order to investigate the scope of activity of the Ru/PVPy catalyst, the hydrogenation of a series of other monocyclic and polycyclic aromatic hydrocarbons (MAHs and PAHs) representative of components of petroleum-derived fuels was carried out under moderate conditions. As summarized in Table 1, Ru/PVPy is effective for the hydrogenation of a variety of monocyclic arenes at 120 °C under 10 bar. The hydrogenation rate decreases with increasing steric congestion

on the arene ring; a comparison of entries 1–6 shows a steady decrease in the TOF values from 120 h⁻¹ for benzene to 3 h⁻¹ for mesitylene. On the other hand, the hydrogenation rate is rather insensitive to electronic effects, as revealed by comparison of entries 2, 8 and 9, where the presence of the electron-withdrawing substituent –CF₃ and the electron-donating –OCH₃ on the ring produces only a moderate deactivating effect. This is consistent with Dupont's work on Ru nanoparticles immobilized in ionic liquids, where relative reaction rates were found to be dominated by steric factors.¹³ Benzene and toluene are exclusively hydrogenated to the corresponding cyclohexanes (Table 1, entries 1 and 2), but the more resistant substrates yield mixtures of cycloalkenes and cycloalkanes, with the latter being the major products; the cyclohexenes formed are those with the more highly substituted double bond (Table 1, entries 3–9). As expected, an increase in temperature and pressure increased the hydrogenation rates for MAHs, raising the TOF value, in the case of mesitylene, from 3 h⁻¹ at 120 °C and 10 bar to 40 h⁻¹ at 150 °C and 40 bar (Table 1, entries 6 and 7). The proportion of fully hydrogenated product also increased at higher temperatures and pressures or at longer reaction times.

Bicyclic and tricyclic aromatic hydrocarbons, which are generally difficult to reduce, were also hydrogenated efficiently over Ru/PVPy (Table 2). Trace amounts of S in commercial

Table 2 Hydrogenation of polycyclic aromatic hydrocarbons (PAHs) over Ru/PVPy^a

Substrate	TOF (h ⁻¹)	Product distribution at 1 h
	60	 78%  2%  20%
	45 ^b	 77%  11%  7%  4%  1%

^a In THF; $n_{\text{sub}} : n_{\text{Ru}} = 100$; 150 °C, 50 bar H₂; ^b $n_{\text{sub}} : n_{\text{Ru}} = 50$.

naphthalene and anthracene (0.2% benzothiophene and 0.3% dibenzothiophene, respectively) were found to poison our Ru/PVPy catalyst; consequently, the use of these substrates as received resulted in very low rates (TOF < 10 h⁻¹) even at 150 °C and 50 bar H₂. Attempts to remove the S-aromatic impurities from naphthalene or anthracene by recrystallization, sublimation or chromatography were unsuccessful; therefore, Ru/PVPy itself was used to trap the S-containing molecules as an alternative strategy to purify the substrate.

In the case of naphthalene, 100 mg of Ru/PVPy was used as a sacrificial catalyst to treat 1.28 g of naphthalene at 120 °C under 20 bar H₂. The amount of benzothiophene was monitored by gas chromatography as the reaction proceeded and upon complete disappearance of benzothiophene, the reaction was stopped. The sacrificial catalyst was removed, 100 mg of fresh catalyst was then added to the pretreated naphthalene solution and the hydrogenation reaction was started again. The catalytic rates increased considerably on the pure substrates; naphthalene was hydrogenated mainly to 1,2,3,4-tetrahydronaphthalene, with minor amounts of decahydronaphthalene and traces of octahydronaphthalene, with a TOF of 60 h⁻¹. Anthracene was hydrogenated to 1,2,3,4-tetrahydroanthracene as the major product, along with several other minor hydrogenation products, with a TOF of 40 h⁻¹, as shown in Table 2. PAHs, as expected, are more resistant to hydrogenation than MAHs, thus requiring higher temperature and pressure to obtain comparable rates with those of MAHs. The outer rings of the tricyclic arene are hydrogenated more easily than the inner benzene ring, as shown in the product distribution for the hydrogenation of anthracene. Hydrogenation of naphthalene and anthracene has been observed over Ru particles supported on polyorganophosphazenes¹⁸ and on silica,²³ but we are not aware of any other reports on hydrogenation of PAHs by Ru nanoparticles.

2.3.2. Hydrogenation of N-heteroaromatic compounds. N-heteroaromatic compounds are present in petroleum and accumulate from the blending of straight run distillates and cracked products of heavier feedstocks with a high nitrogen content;⁵⁰ they are mainly in the form of basic (pyridine, acridine and quinoline) and neutral (indol and carbazole) compounds, and are of great concern not only because they contribute NO_x emissions but also because they commonly act as catalyst poisons, by strong adsorption on the active sites of catalysts.

2.3.2.1. Hydrogenation of quinoline. Ru/PVPy can hydrogenate quinoline under moderate reaction conditions, as depicted in Fig. 8. The reaction profile in Fig. 8a indicates that at 120 °C and 10 bar H₂, the heterocyclic ring is reduced preferentially, with only small amounts of product resulting from hydrogenation of the carbocyclic ring (Table 3, entry 7). Under 150 °C and 50 bar H₂ a TOF of 171 h⁻¹ is achieved (Table 3, entry 8). In contrast with the case of toluene, the effect of H₂ pressure on catalytic activity displays a “volcano” relationship (Fig. 8b), with a maximum around 40 bar at 120 °C. Some of these data have been previously disclosed in a preliminary communication.⁴³ Only a few other supported Ru catalysts are known to hydrogenate N-aromatics: Spitaleri *et al.* reported the reduction of quinoline by Ru NPs on polyorganophosphazenes in homogeneous phase, with a TOF of about 170 h⁻¹ at 25 °C and 50 bar H₂;¹⁸ Bianchini and coworkers

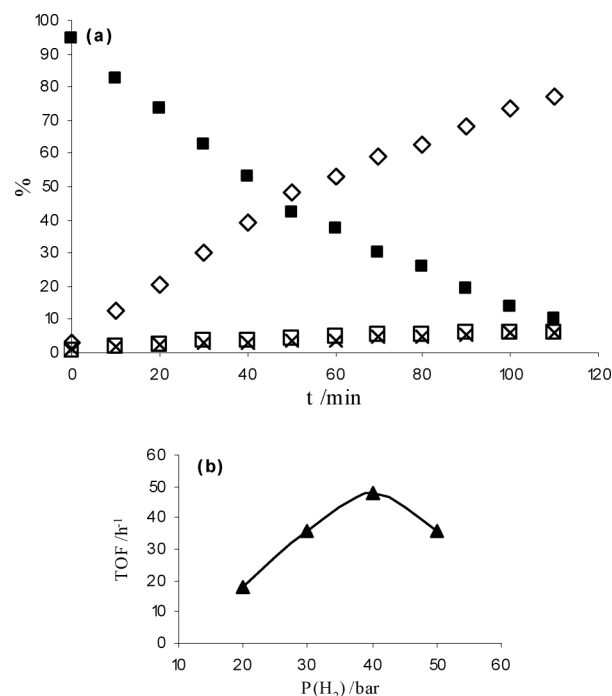
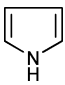
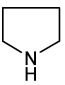

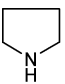
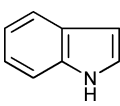
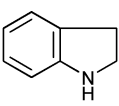
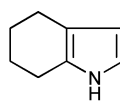
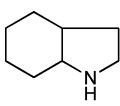
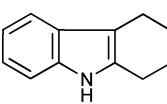
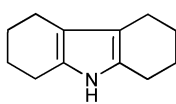
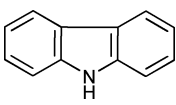
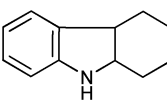
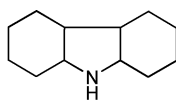
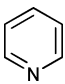
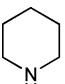
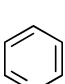

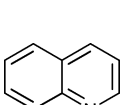
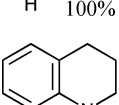
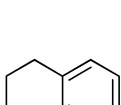
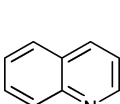
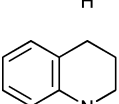
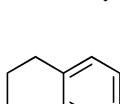
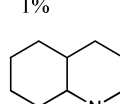
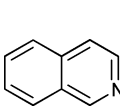
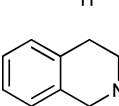
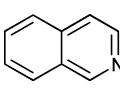
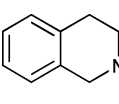


Fig. 8 (a) Hydrogenation of quinoline over Ru/PVPy (120 °C, 40 bar H₂; $n_{\text{Q}} : n_{\text{Ru}} = 84$; in toluene; ■: Q; ◇: N-THQ; □: C-THQ; ×: DHQ); (b) effect of H₂ pressure on hydrogenation rate (120 °C; $n_{\text{Q}} : n_{\text{Ru}} = 84$; in toluene).

Table 3 Hydrogenation of selected N-heteroaromatics over Ru/PVPy

Entry	Substrate	$T/^{\circ}\text{C}$	P_{H_2} (bar)	TOF (h^{-1})	Product distribution at 1 h
1		120	30	4	 100%
2		150	50	71	 100%
3		150	50	45	 +  25%  75%
					 77%  15%
4		150	50	22	 1%  7%
5		120	10	12	 100%
6		150	50	101	 100%
7		120	10	19	 99%  1%
8		150	50	171	 29%  17%  54%
9		150	30	14	 100%
10		150	50	28	 100%

used silica-supported Ru particles to hydrogenate quinoline to a mixture of products at 100 °C and 30 bar H_2 with a TOF of about 100 h^{-1} .²³ Li and coworkers used a hydroxyapatite-supported Ru catalyst for hydrogenation of quinoline and some of its methylated derivatives at 150 °C and 40 bar with TOF values of the order of 200 h^{-1} .³¹

2.3.2.2. Hydrogenation of other N-heteroaromatics. Ru/PVPy is also efficient for the hydrogenation of a variety of other N-heteroaromatic compounds representative of fuel components under moderate conditions (150 °C and 30/50 bar H_2), as summarized in Table 3. Pyridine and quinoline were easily

reduced at 120 °C under 10 bar (Table 3, entries 5 and 7), while hydrogenation of pyrrole and other five-membered N-heterocycles required higher temperatures and pressures (150 °C and 50 bar H_2 , Table 3, entries 1–4). Interestingly, quinoline is more easily hydrogenated than isoquinoline under the same conditions but less selectively (Table 3, entries 8 and 10); specific reduction of the heterocyclic ring was observed even when both the temperature and the pressure were increased (Table 3, entries 9 and 10), in contrast to the case of quinoline (Table 3, entries 7 and 8). There are, to our knowledge, no other reports on such versatility in the hydrogenation of

Table 4 Reutilization of Ru/PVPy

Substrate	Cycle	TOF (h ⁻¹)
toluene ^a	1	400
	2	550
	3	545
quinoline ^b	1	19
	2	24
	3	19

^a Tol: 25 cm³; cat.: 231 mg; solventless; 120 °C, 20 bar; ^b Q: 1 cm³; cat.: 84 mg; solvent: THF; 120 °C, 10 bar.

N-heteroaromatic compounds catalyzed by supported Ru nanoparticles.

2.3.3. Catalyst recyclability. The recyclability of Ru/PVPy was established by using the same catalyst sample in three consecutive hydrogenation runs of either neat toluene or quinoline in THF. The catalyst was carefully recovered under a nitrogen atmosphere and re-used in subsequent cycles. As shown in Table 4, the TOF values for both toluene and quinoline hydrogenation displayed very little variation in consecutive runs. Consistently, the average Ru particle size was only moderately increased after the first toluene hydrogenation run (Fig. S1, ESI†) and no important further changes in particle size distribution were observed by TEM after three consecutive hydrogenation runs.

2.4. Insights into possible reaction mechanisms

Supported metal catalysts most commonly operate by homolytic hydrogen activation and transfer of atomic hydrogen to chemisorbed substrate molecules (eqn (1)). Catalyst poisoning frequently occurs in the presence of *e.g.* N-heterocycles due to strong adsorption of the substrate and/or of their hydrogenation products on the active metal sites. Our catalyst design involves metallic nanoparticles intimately associated with a basic support, with the aim of creating a nanostructure capable of promoting the heterolytic activation of hydrogen and ionic hydrogenation mechanisms (eqn (2)), as a strategy to avoid catalyst poisoning. In this context, the support not only stabilizes the Ru nanoparticles, but may also become directly involved in the catalytic reactions. In order to gain some insight into the principal mechanisms operating in the hydrogenation reactions studied, the following experiments were conducted:

2.4.1. Solvent effects. The hydrogenation of toluene or quinoline was carried out in the presence of a variety of solvents. The results of those experiments, depicted in Fig. 9, indicate a correlation between higher solvent polarity and higher catalytic activity in the case of quinoline (Fig. 9a),⁴³ in agreement with an ionic mechanism. For toluene, on the other hand, there is no relation between TOF values and solvent polarity (Fig. 9b), indicating a classical homolytic pathway.

2.4.2. Effect of adding external acid or base. A TOF enhancement from 66 h⁻¹ to 120 h⁻¹ was observed for the hydrogenation of quinoline (120 °C, 30 bar H₂, in methanol) upon addition of the strong base Et₃N (10 eq), which can be related to heterolytic H₂ splitting; this is a common activation pathway in homogeneous catalysis, *e.g.* for RuCl₂(PPh₃)₃, which readily reacts with H₂ in the presence of the amine to yield the active hydride RuHCl(PPh₃)₃ +

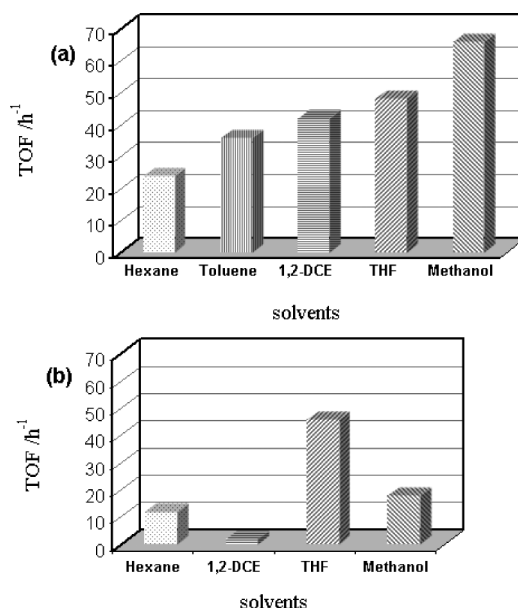


Fig. 9 Effect of solvent on the hydrogenation of (a) quinoline (120 °C, 30 bar H₂; $n_Q : n_{Ru} = 84$; in toluene) and (b) toluene (120 °C, 10 bar H₂; $n_{Tol} : n_{Ru} = 100$; in THF) over Ru/PVPy.

Et₃N·HCl.³⁷ The heterolytic splitting mechanism envisaged for our catalysts in the case of the N-heteroaromatics could be initiated by either the basic pyridine groups of the support, or by the basic substrates themselves. In either case, protonation of the N atom of the substrate would be assisted by hydrogen bonding to the N atom of a pyridine group in the support (Fig. 10). Addition of HBF₄ (10 eq) also produced an increase in TOF to 180 h⁻¹ under the same conditions, most likely due to protonation of the pyridine groups of the support or of the substrate, leading to the same type of hydrogen bonded intermediate on the surface.

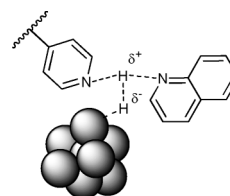


Fig. 10 Heterolytic splitting of H₂ assisted by the support on Ru/PVPy catalysts.

On the other hand, in the case of toluene hydrogenation, addition of Et₃N did not have a noticeable effect on the TOF, while addition of HBF₄ had a deleterious effect. This is in accord with a homolytic pathway, since a proportion of the adsorbed H atoms on the metal active sites would react with H⁺ to release hydrogen gas and would therefore not be available for transfer to the substrate.

2.4.3. Substrate competition and selective poisoning experiments. Substrate competition experiments were performed at 150 °C and 50 bar of H₂, using equimolar amounts of toluene and quinoline, while keeping the total substrate to Ru molar ratio at 100 : 1. The reaction profile is depicted in Fig. 11. At the early stages of hydrogenation (30 min), only quinoline was reduced with a TOF of 156 h⁻¹, predominantly at the heterocyclic ring to yield

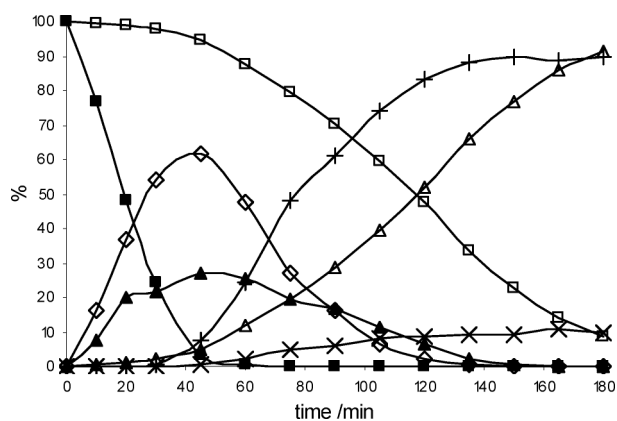


Fig. 11 Hydrogenation profile of equimolar quinoline and toluene (150 °C, 50 bar H₂; $n_Q : n_{Tol} : n_{Ru} = 100 : 100 : 1$; in THF; ■: Q; ◇: *N*-THQ; ▲: *C*-THQ; +: *trans*-DHQ; ×: *cis*-DHQ; □: Tol; △: methylcyclohexane).

1,2,3,4-tetrahydroquinoline (*N*-THQ) but also at the carbocyclic ring to produce 5,6,7,8-tetrahydroquinoline (*C*-THQ) as a minor product (25%); at longer reaction times (>45 min), both *N*-THQ and *C*-THQ were further reduced to *cis/trans* decahydroquinoline (DHQ), the former at a more pronounced rate. Toluene, on the other hand, was only hydrogenated to an important degree after all the quinoline and most of the THQ had been consumed; this observation indicates that the presence of quinoline, and to a lesser extent *N*-THQ inhibited the hydrogenation of toluene.

This suggests the possibility of two different hydrogenation mechanisms acting in parallel on two distinct sites on the Ru/PVPy catalyst, as illustrated in Fig. 12: The first involves heterolytic hydrogen splitting and ionic hydrogenation of *polar N-heteroaromatics* (path *a*) taking place at Type A sites, while the second one (path *b*) operates for *non-polar aromatics* and most likely involves conventional homolytic hydrogen splitting on Type B sites. Quinoline would thus be hydrogenated simultaneously at the heterocyclic ring at Type A sites through pathway *a* to produce *N*-THQ and at the carbocyclic ring at Type B sites through pathway *b* to give *C*-THQ; these parallel reactions on quinoline would block the access of toluene to the B type sites. Once quinoline and most of the THQ are consumed, toluene

can effectively compete for the Type B sites and be hydrogenated through path *b* to methylcyclohexane.

Further evidence for the proposed dual site mechanism on Ru/PVPy was obtained from selective poisoning caused by addition of small amounts of thiophene. In a poisoning test, 10 µL of thiophene was mixed into 1 cm³ of quinoline ($n_Q : n_S : n_{Ru} = 100 : 1.5 : 1$) prior to the hydrogenation run. At 150 °C and 50 bar H₂, quinoline was exclusively hydrogenated to *N*-THQ, with an initial TOF value of 161 h⁻¹, essentially the same as for the substrate competition experiment. There was no evidence for the formation of even traces of *C*-THQ or DHQ; this implies that thiophene selectively blocks Type B sites (and consequently pathway *b*) for the hydrogenation of the carbocyclic ring of quinoline but has no effect on the hydrogenation of the heterocyclic ring.

On the other hand, when toluene was used as the substrate, the presence of small amounts of thiophene fully inhibited the hydrogenation reaction. Thiophene was not hydrogenated in either case. An explanation consistent with all the details extracted from our combined results is that carbocyclic rings (of quinoline or toluene) are hydrogenated at type B sites in Ru/PVPy, through a homolytic hydrogen splitting pathway *b*, but thiophene binds strongly to such sites, effectively poisoning their catalytic activity. *N*-heterocyclic rings, in contrast, are hydrogenated at type A sites through an ionic mechanism *a*, involving the heterolytic splitting of H₂ assisted by the basic support; thiophene probably has little or no affinity for this type of site and thus the only effect of thiophene on the hydrogenation of quinoline is to suppress the hydrogenation of the carbocyclic ring at type B sites and drive the selectivity for *N*-THQ to 100%.

3. Conclusions

We have designed and synthesized a new nanostructured catalytic material composed of Ru nanoparticles immobilized on the basic polymer poly(4-vinylpyridine). TEM measurements show the Ru nanoparticles are well-dispersed and the size does not change appreciably after a hydrogenation run. Powder XRD diffraction patterns and XPS measurements confirm that the nanoparticles

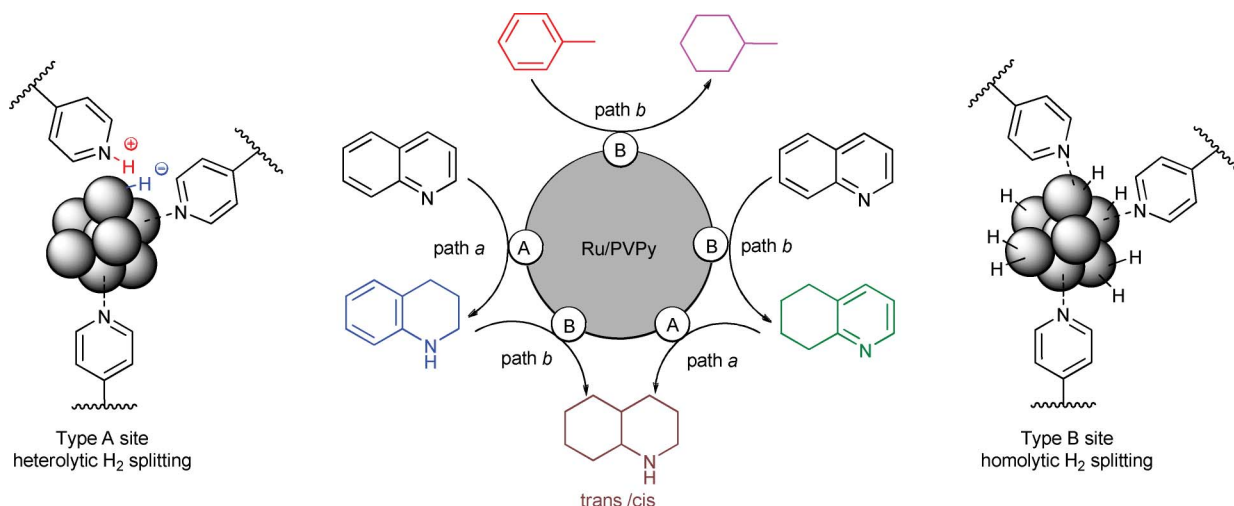


Fig. 12 The model of the dual-site structure of Ru/PVPy catalyst and the corresponding hydrogenation pathways.

are predominantly Ru metal. The new material is a versatile catalyst for the hydrogenation of a variety of mono- and polycyclic arenes and N-heteroaromatics representative of components of petroleum-derived fuels. The effect of solvent polarity and addition of external acid or base, substrate competition experiments and selective thiophene poisoning tests strongly suggest that the catalyst has two distinct active sites and is therefore capable of functioning through two parallel mechanisms, one of which is an ionic mechanism involving heterolytic hydrogen splitting, an extremely rare pathway on metallic surfaces.

4. Experimental

4.1. Materials

Ruthenium trichloride hydrate (Pressure Chemicals, Inc.) was used as received. Solvents (analytical grade, Sigma-Aldrich) were purified using a PureSolv purification unit from Innovative Technology, Inc. Substrates and other reagents (Sigma-Aldrich) were purified by distillation or recrystallization prior to use when necessary. Poly(4-vinylpyridine) (2% cross-linked with divinylbenzene) was purchased from Sigma-Aldrich and dried under vacuum at 50 °C overnight before use.

4.2. Catalyst synthesis

The Ru/PVPy catalyst was synthesized by NaBH_4 reduction of $\text{RuCl}_3 \cdot 3\text{H}_2\text{O}$ in the presence of poly(4-vinylpyridine) in methanol under nitrogen. The reaction is performed in a three-neck round bottom flask fitted with two pressure-equalizing dropping funnels and a reflux condenser. Using Schlenk techniques, the apparatus was evacuated and purged with nitrogen three times. Poly(4-vinylpyridine) (1.0 g) was suspended in methanol (20 cm^3) inside the flask under nitrogen; $\text{RuCl}_3 \cdot 3\text{H}_2\text{O}$ (0.26 g, containing 0.10 or 1.0 mmol of Ru) in methanol (10 cm^3) and NaBH_4 (0.38 g, 10 mmol) in methanol (20 cm^3) were placed in the two dropping funnels, respectively. While the polymer suspension was being stirred at room temperature, 10 cm^3 of the NaBH_4 solution was quickly added to the flask, after which both RuCl_3 and NaBH_4 solutions were simultaneously added into the mixture at the same rate of about one drop per second. After addition was complete, the mixture was further stirred for 2 h at room temperature. At the end, the solution was colorless and the solid was dark brown. The solid was filtered off, washed three times with deionized water (10 cm^3) and three times with methanol (10 cm^3) and dried under vacuum at room temperature, affording a fine brown powder containing 10 wt% Ru.

4.3. TEM studies

Transmission electron microscopy (TEM) micrographs were obtained on a Zeiss EM 902 microscope operating at an accelerating voltage of 80 kV with a line resolution of 0.34 nm and a point resolution of 0.5 nm. Images were captured digitally using a Mega View III CCD camera with a resolution of 1.3 megapixels. The metal particle size (Feret diameter) distribution was estimated from the measurement of about 300 particles, found in an arbitrarily chosen area in an enlarged micrograph.

TEM samples were prepared as follows: about 50 mg of catalyst was ground in a mortar and subsequently mixed with M bond 610

two-part epoxy (E.A. Fischione Instruments, Inc., part A : part B = 10 : 1). The mixture was transferred into a 3 mm brass tube and then cured at 150 °C for 40 min. A disk of about 500 μm thickness was cut off from the filled brass tube using an IsoMet® low speed diamond wafering saw (Buehler) and then mechanically pre-thinned to about 200 μm thick on an EcoMet® variable speed grinder-polisher (Buehler). The disk was further polished by dimple grinding on a Model 200 dimpling grinder (E.A. Fischione Instruments, Inc.) to about 10 μm in the central area. The final sample was prepared by dual gun Ar^+ ion milling in a Fischione Model 1010 low angle ion milling and polishing system to reach a perforation in the central area of the dimple ground disk. A summary of this procedure is illustrated in Scheme S1, ESI.†

4.4. XRD measurements

Powder X-ray diffraction (XRD) patterns were recorded on a Philips X'PERT MPD diffractometer using monochromatic $\text{Cu-K}\alpha$ radiation at 45 kV and 40 mA and 2θ scanning from 10° to 75°. Samples were ground in a mortar before being placed in a sample holder and analyzed immediately in air at room temperature.

4.5. XPS measurements

XPS spectra were recorded with an Omicron XPS spectrometer equipped with a multichannel hemispherical analyzer and a dual Al/Mg X-ray source using Al $\text{K}\alpha$ excitation (1486.6 eV). The binding energy scale was previously calibrated and the base pressure in the analysis chamber was around 2.0×10^{-9} torr. The powdered samples were mounted on studs using a double-sided adhesive tape with a short time of air exposure. The pressure in the analysis chamber was maintained below 5.0×10^{-8} torr during the measurements. The asymmetrical XPS peaks were deconvoluted by the curve fitting approach by use of XPSPEAK 4.1, applying Shirley background subtraction and Lorentzian-Gaussian functions (20% L, 80% G).

4.6. Catalytic tests

Experiments were carried out using a 5513 Parr reactor (100 cm^3) fitted with an internal stirrer and a dip tube, a thermocouple, a sampling valve and a high-pressure burette, coupled to a 4836 controller. In a typical hydrogenation run, the reactor was loaded with the desired amount of the catalyst and 20 cm^3 of solvent and then sealed. H_2 was introduced into the reactor through the high-pressure burette and released three times in order to deoxygenate the system, after which the reactor was re-pressurized to 6 bar and heated to 120 °C to reach 10 bar. After the catalyst was incubated at 120 °C under 10 bar for 1 h, 1 cm^3 of liquid substrate dissolved in 10 cm^3 of the same solvent was placed into the high-pressure burette, which was subsequently charged with 10 bar of H_2 . The reactor was depressurized to about 2–3 bar and the substrate in the burette was then quickly injected into the reactor. The pressure was adjusted to the desired value (this was taken as the zero time of the reaction) and kept constant by feeding through an open connection to the hydrogen tank. Samples of the reaction mixture were periodically withdrawn from the reactor and analyzed immediately by use of a Varian 3900 gas chromatograph fitted with a FactorFour VF-5ms capillary column and a Saturn 2100T mass detector. The identity of each

product was verified through comparison of its mass spectrum with the instrument's library and the molar percentage of each product was calculated based on peak areas, previously calibrated by using a series of standard solutions containing known amounts of each component. Each experiment was repeated at least twice in order to verify reproducibility; the variations in the calculated TOF values for repeat experiments were typically within 10%.

4.7. Substrate competition experiments

The procedure for substrate competition experiments was analogous to the one described in section 4.6, except that the two substrates (toluene and quinoline) in equimolar amounts were placed in the high-pressure burette.

4.8. Selective thiophene poisoning tests

The procedure for selective poisoning experiments was analogous to the one described in section 4.6, except that the substrate (toluene or quinoline) was mixed with thiophene (~1 mol%) before being placed in the high-pressure burette.

4.9. Recycling experiments

A hydrogenation run was performed as described in section 4.6. At the end of the reaction, the reactor was allowed to cool to room temperature, vented, opened and the mixture was completely transferred into a Schlenk flask under a nitrogen atmosphere. The supernatant liquid was carefully withdrawn by use of a syringe, 10 cm³ of deoxygenated solvent was added and the mixture was then stirred for five minutes. This procedure was repeated three times. At the end, the residual solvent was removed and the catalyst was dried under vacuum for 2 h. A second hydrogenation run was then performed with this catalyst; further recycling steps were carried out by repeating this procedure.

Acknowledgements

We thank Dr Nim Lal Nakarmi and Cai Bo (Physics Department) for assistance in preparing samples for TEM and Dr Zhongqi Cheng (Geology Department) for assistance with XRD measurements, both through the Environmental Sciences Analytical Center (ESAC) of Brooklyn College, and Drs. Alan Lyons and Qianfeng Xu (Chemistry Department, College of Staten Island, CUNY) for assistance and use of their XPS instrument. Acknowledgement is made to the Donors of the American Chemical Society Petroleum Research Fund and to the US Department of Energy for support of this research through Grants 47472-AC3 and DE-EE0003129, respectively.

Notes and references

- 1 <http://www.energy.gov/energysources/fossilfuels.htm> (accessed 2011).
- 2 H. Topsøe, B. S. Clausen and F. E. Massoth, *Hydrotreating Catalysis, Science and Technology*, Springer-Verlag, Heidelberg, 1996.
- 3 J. G. Speight, *The Desulfurization of Heavy Oils and Residua*, Marcel Dekker, New York, 2000.
- 4 R. A. Sánchez-Delgado, *Organometallic Modeling of the Hydrodesulfurization and Hydrodenitrogenation Reactions*, Kluwer, Dordrecht, 2002.
- 5 P. Tian, J. Blanchard, K. Fajeweg, M. Breyse, M. Vrinat and Z. Liu, *Microporous Mesoporous Mater.*, 2003, **60**, 197–206.
- 6 G. Schmid, Ed., *Nanoparticles: From Theory to Application*, Wiley-VCH, Weinheim, 2004.
- 7 D. Astruc, F. Lu and J. R. Aranzaes, *Angew. Chem., Int. Ed.*, 2005, **44**, 7852–7872.
- 8 A. Gual, C. Godard, S. Castillón and C. Claver, *Dalton Trans.*, 2010, **39**, 11499–11512.
- 9 P. S. Campbell, C. C. Santini, D. Bouchu, B. Fenet, K. Philippot, B. Chaudret, A. A. H. Padua and Y. Chauvin, *Phys. Chem. Chem. Phys.*, 2010, **12**, 4217–4223.
- 10 L. M. Rossi and G. Machado, *J. Mol. Catal. A: Chem.*, 2009, **298**, 69–73.
- 11 M. H. G. Precht, M. Scariot, J. D. Scholten, G. Machado, S. R. Teixeira and J. Dupont, *Inorg. Chem.*, 2008, **47**, 8995–9001.
- 12 A. Nowicki, V. Le Boulair and A. Roucoux, *Adv. Synth. Catal.*, 2007, **349**, 2326–2330.
- 13 G. S. Fonseca, E. T. Silveira, M. A. Gelesky and J. Dupont, *Adv. Synth. Catal.*, 2005, **347**, 847–853.
- 14 K. Pelzer, O. Vidoni, K. Philippot, B. Chaudret and V. Collière, *Adv. Funct. Mater.*, 2003, **13**, 118–126.
- 15 (a) A. Gual, C. Godard, K. Philippot, B. Chaudret, A. Denicourt-Nowicki, A. Roucoux, S. Castillón and C. Claver, *ChemSusChem*, 2009, **2**, 769–779; (b) A. Gual, M. R. Axet, K. Philippot, B. Chaudret, A. Denicourt-Nowicki, A. Roucoux, S. Castillón and C. Claver, *Chem. Commun.*, 2008, 2759–2761.
- 16 A. Denicourt-Nowicki, A. Ponchel, E. Monflier and A. Roucoux, *Dalton Trans.*, 2007, 5714–5719.
- 17 L. Song, X. Li, H. Wang, H. Wu and P. Wu, *Catal. Lett.*, 2009, **133**, 63–69.
- 18 A. Spitaleri, P. Pertici, N. Scalera, G. Vitulli, M. Hoang, T. W. Turney and M. Gleria, *Inorg. Chim. Acta*, 2003, **352**, 61–71.
- 19 F. Su, L. Lv, F.-Y. Lee, T. Liu, A. I. Cooper and X.-S. Zhao, *J. Am. Chem. Soc.*, 2007, **129**, 14213–14223.
- 20 J. Ning, J. Xu, J. Liu and F. Lu, *Catal. Lett.*, 2006, **109**, 175–180.
- 21 J. Huang, T. Jiang, B. Han, W. Wu, Z. Liu, Z. Xie and J. Zhang, *Catal. Lett.*, 2005, **103**, 59–62.
- 22 G. Marconi, P. Pertici, C. Evangelisti, A. M. Caporusso, G. Vitulli, G. Capannelli, M. Hoang and T. W. Turney, *J. Organomet. Chem.*, 2004, **689**, 639–646.
- 23 C. Bianchini, V. D. Santo, A. Meli, S. Moneti, M. Moreno, W. Oberhauser, R. Psaro, L. Sordelli and F. Vizza, *J. Catal.*, 2003, **213**, 47–62.
- 24 X. Zhou, T. Wu, B. Hu, T. Jiang and B. Han, *J. Mol. Catal. A: Chem.*, 2009, **306**, 143–148.
- 25 S. Boujday, J. Blanchard, R. Villanneau, J.-M. Krafft, C. Geantet, C. Louis, M. Breyse and A. Proust, *ChemPhysChem*, 2007, **8**, 2636–2642.
- 26 M. Zahmakiran, Y. Tonbul and S. Özkaz, *Chem. Commun.*, 2010, **46**, 4788–4790.
- 27 M. Zahmakiran, Y. Tonbul and S. Özkaz, *J. Am. Chem. Soc.*, 2010, **132**, 6541–6549.
- 28 M. Zahmakiran and S. Özkaz, *Langmuir*, 2008, **24**, 7065–7067.
- 29 M. Takasaki, Y. Motoyama, K. Higashi, I. Mochida and H. Nagashima, *Chem.-Asian J.*, 2007, **2**, 1524–1533.
- 30 F. Su, F.-Y. Lee, L. Lv, J. Liu, X.-N. Tian and X.-S. Zhao, *Adv. Funct. Mater.*, 2007, **17**, 1926–1931.
- 31 Y. Sun, H. Fu, D. Zhang, R. Li, H. Chen and X. Li, *Catal. Commun.*, 2010, **12**, 188–192.
- 32 C.-W. Chiang, A. Wang, B.-Z. Wan and C.-Y. Mou, *J. Phys. Chem. B*, 2005, **109**, 18042–18047.
- 33 V. Rao, P. A. Simonov, E. R. Savinova, G. V. Plaksin, S. Cherepanova, G. Kryukova and U. Stimming, *J. Power Sources*, 2005, **145**, 178–187.
- 34 Y. V. Larichev, B. L. Moroz, V. I. Zaikovskii, S. M. Yunusov, E. S. Kalyuzhnaya, V. B. Shur and V. I. Bukhtiyarov, *J. Phys. Chem. C*, 2007, **111**, 9427–9436.
- 35 G. C. Bond, *Catalysis by Metals*, Academic Press, New York, 1962.
- 36 G. C. Bond, *Metal-Catalysed Reactions of Hydrocarbons*. In *Fundamental and Applied Catalysis*, M. V. Twigg and M. S. Spencer, ed., Springer, New York, 2005.
- 37 R. H. Crabtree, *The Organometallic Chemistry of the Transition Metals*, 5th Ed., Wiley-Interscience, Hoboken, NJ, 2009.
- 38 R. Noyori and T. Ohkuma, *Pure Appl. Chem.*, 1999, **71**, 1493–1501.
- 39 R. Noyori and T. Ohkuma, *Angew. Chem., Int. Ed.*, 2001, **40**, 40–73.
- 40 C. A. Sandoval, T. Ohkuma, K. Muñiz and R. Noyori, *J. Am. Chem. Soc.*, 2003, **125**, 13490–13503.
- 41 M. Breyse, E. Furimsky, S. Kasztelan, M. Lacroix and G. Perot, *Catal. Rev. Sci. Eng.*, 2002, **44**, 651–735.

- 42 M. Lacroix, S. Yuan, M. Breyse, C. Dorémieux-Morin and J. Fraissard, *J. Catal.*, 1992, **138**, 409–412.
- 43 R. A. Sánchez-Delgado, N. Machalaba and N. Ng-a-qui, *Catal. Commun.*, 2007, **8**, 2115–2118.
- 44 W. F. McClune, Ed., *Powder Diffraction File, Inorganic Phases*, Card # 6-0663, JCPDS International Centre for Diffraction Data, Swarthmore, PA, 1988.
- 45 J. F. Moulder, W. F. Stickle, P. E. Sobol and K. D. Bomben, Eds, *Handbook of X-ray Photoelectron Spectroscopy: A Reference Book of Standard Spectra for Identification and Interpretation of XPS Data*, Perkin-Elmer, Eden Prairie, MN, 1992.
- 46 G. Beamson and D. Briggs, *High Resolution XPS of Organic Polymers: The Scienta ESCA300 Database*, John Wiley & Sons, Chichester, UK, 1992.
- 47 K. Aika, J. Kubota, Y. Kadowaki, Y. Niwa and Y. Izumi, *Appl. Surf. Sci.*, 1997, **121–122**, 488–491.
- 48 S. Dahl, A. Logadottir, C. J. H. Jacobsen and J. K. Nørskov, *Appl. Catal., A*, 2001, **222**, 19–29.
- 49 J. C. Fuggle, T. E. Madey, M. Steinkilberg and D. Menzel, *Surf. Sci.*, 1975, **52**, 521–541.
- 50 Y. Briker, Z. Ring, A. Iachelli and N. Mc Lean, *Fuel*, 2003, **82**, 1621.